

Skip-WaveNet: A Wavelet based Multi-scale Architecture to Trace Firn Layers in Radar Echograms

Debvrat Varshney, *Student Member, IEEE*, Masoud Yari, *Member, IEEE*,
Oluwanisola Ibikunle, *Student Member, IEEE*, Jilu Li, *Senior Member, IEEE*, John Paden, *Member, IEEE*,
Maryam Rahnemoonfar, *Member, IEEE*

Abstract—Echograms created from airborne radar sensors capture the profile of firn layers present on top of an ice sheet. Accurate tracking of these layers is essential to calculate the snow accumulation rates, which are required to investigate the contribution of polar ice cap melt to sea level rise. However, automatically processing the radar echograms to detect the underlying firn layers is a challenging problem. In our work, we develop wavelet-based multi-scale deep learning architectures for these radar echograms to improve firn layer detection. We show that wavelet based architectures improve the optimal dataset scale (ODS) and optimal image scale (OIS) F-scores by 3.99% and 3.7%, respectively, over the non-wavelet architecture. Further, our proposed Skip-WaveNet architecture generates new wavelets in each iteration, achieves higher generalizability as compared to state-of-the-art firn layer detection networks, and estimates layer depths with a mean absolute error of 3.31 pixels and 94.3% average precision. Such a network can be used by scientists to trace firn layers, calculate the annual snow accumulation rates, estimate the resulting surface mass balance of the ice sheet, and help project global sea level rise.

Index Terms—Wavelet transforms, multi-scale architectures, contour detection, firn layer tracking, convolutional neural networks, sea-level rise

I. INTRODUCTION

Increase of global mean annual temperature every year is having a drastic effect on the polar ice-caps. Intergovernmental Panel on Climate Change (IPCC) 2021 report [1] states that the Arctic has warmed at more than twice the global rate over the past 50 years, and the melting of the Greenland Ice Sheet (GrIS) will cause sea levels to rise by 2 meters by 2100, potentially flooding regional coastal areas [2]. Hence, accurate projections of sea level rise are required to prepare us for future natural disasters. Modern climate models that simulate and project sea level rise rely on the rates at which the polar ice caps accumulate snow, as well as drainage from their glaciers. Continuous monitoring and evaluation of the

changing ice sheets is hence imperative to support climate models make accurate projections.

Polar ice sheets are thick masses of ice, on top of which snow gets accumulated every year to form ‘snow accumulation layers’, also known as ‘firn layers’ [3]. The accumulation of, and melt from, these firn layers changes the surface mass balance of the ice sheet and contributes to sea level increase. Airborne radar systems such as the Snow Radar [4] monitor and capture the internal state of these firn layers annually. Significant variations in snow permittivity reflect the electromagnetic signals transmitted by Snow Radar. This reflection, which can be seen as the layers in radar echograms, often occurs at the boundaries of snow stratigraphy, where changes in the physical properties of the snow, such as density, hardness, grain size and shape, result in significant discontinuities in the snow’s dielectric properties. However, the visibility and clarity of the firn layers in Snow Radar echograms will degrade when the magnitude of the discontinuity in the snow’s dielectric properties decreases. Routine data processing has applied deconvolution, filtering, coherent and incoherent integration techniques to remove non-ideal system characteristics and improve signal-to-noise ratio; however, off-nadir surface backscattering, multipath scattering, and signal loss in the medium may still exacerbate the degradation of Snow Radar echogram’s quality (see the examples in the leftmost columns of Figures 8-10).

We collectively refer to the above degradation phenomena as “noise”. This noise makes tracking accumulation layers challenging even for experienced glaciologists and significantly increases the workload for conventional vision algorithms [3], [5]. Even convolutional neural networks (CNNs) [6], which have become the standard machine learning algorithms for image processing, have issues in making accurate predictions from these images [5], [7], [8] since any interruptions to their input can drastically affect their prediction capability [9]. Further, as the radar images are noisy, visually picking the layers for manual annotations either creates missing or incomplete labels for most firn layers in these images [3]. Hence, the imperfections in the annotations may mislead the neural networks, which are essentially supervised learning algorithms relying heavily on good quality labelled annotations, into making inaccurate predictions. In this scenario, a possible solution is to have a neural network which can reduce the inherent noise present in images while simultaneously extract-

Manuscript received April 19, 2021; revised August 16, 2021.

This study was supported by NSF BIGDATA awards (IIS-1838230, IIS-1838024), IBM, and Amazon.

Debvrat Varshney is with the Department of Information Systems, University of Maryland Baltimore County, Baltimore, MD 21250, USA.

Masoud Yari and Maryam Rahnemoonfar are with the Department of Computer Science and Engineering at Lehigh University, Bethlehem, PA 18015, USA.

Oluwanisola Ibikunle, Jilu Li and John Paden are with the Center for Remote Sensing and Integrated Systems (CReSIS), University of Kansas, Lawrence, KS 66045, USA.

ing features from them. Such a hybrid architecture would be optimum for highlighting firm layers in radar echograms, which can be used for calculating snow accumulation rates [3], [5].

Wavelet transforms [10] are signal processing techniques that can represent an image in a multi-resolution format and can depict the contextual as well as textural information in the image at different scales [11]. They can decompose a matrix into sparser representations to speed up numerical operations [12], [13]. They also have localization properties, in both the spatial and frequency domains, which can be combined with CNNs to simultaneously learn and remove noise from the input image [10], [14]. These variety of properties have resulted in their applications in image denoising [10], [15], [16], image compression [17], [18], and image restoration [11], [16], [19]. Each level, or scale, of these wavelet transforms is at a downsampled resolution of the previous scale, where the lower scale highlights intricate features and the higher scale emphasizes more global features. Hence, they increase the receptive field size similar to pooling layers of a CNN while additionally avoiding any information loss [9], [16]. On one hand, the CNN filters are made up of weights which are trainable on large datasets mainly through supervised labels, and on the other hand, the filters of a wavelet decomposition are comprised of a fixed basis function which also identifies intrinsic patterns in the input signal. This advantage of wavelet transforms has lead to extensive works which integrate wavelets with CNNs [11], [16], [19]–[21]. [16] performs discrete wavelet transform on convolutional layers in a UNet architecture [22] for image restoration, [20] replaces pooling layers with wavelet transforms to reduce overfitting, and [11] uses wavelet transforms on the input image as well as the embedding net for image super resolution.

In this work, we exploit the multi-scale nature of wavelet transforms and fuse them in a multi-scale convolutional neural network [5] to improve the accuracy of firm layer detection. We also show that taking wavelet transforms of intermediate scales of the neural network helps in learning and extracting features, as compared to taking multi-level wavelet transform of the input image. This work is an extension over our previous workshop paper [23] with a stronger backbone network, more types of wavelet transforms, analysis of ‘static’ wavelets vs ‘dynamic’ wavelets, comparison with state-of-the-art networks, calculation of individual layer depths in terms of number of pixels, along with the use of a more practical Snow Radar dataset.

We highlight the past work on firm layer tracking and wavelet combined neural networks in Section II; give a brief background of wavelet transforms and explain our wavelet based multi-scale architecture(s) in Section III; describe the Snow Radar data that we use for our experiments in Section IV; discuss the quantitative and qualitative results achieved over the Snow Radar data in Section V, and finally conclude the paper in Section VI.

II. RELATED WORKS

Recently, there have been extensive studies on using deep learning for tracking firm layers through noisy radar

echograms. At the same time, wavelet transformations are being exhaustively used to improve the feature extraction capabilities of deep learning networks. Here, we provide a quick overview of the research being done in these two areas.

A. Firm Layer Tracking through Deep Learning

Feature extraction capabilities and good generalizability of deep learning networks have been used on Snow Radar images to track firm layers in [5], [8], [23]–[26]. Deep learning has also been used to segment the radar depth sounder (RDS) images in [27]–[29] into ice and bedrock through various modifications of UNet [22] with or without transformers [30]. In this paper, we focus on the shallow sensor, the Snow Radar, which track the firm layers.

Wang et al. [26] used a CNN-RNN (recurrent neural network) architecture for tiered segmentation of noisy radar images and identifying the top 4-6 firm layers. Similarly, [31] built an iterative neural network architecture to track firm layers, but on simulated radar images, as real radar images were too complex for feature extraction. Authors of [8] used pyramid pooling modules to learn local-to-global spatio-contextual information of firm layer pixels and perform semantic segmentation. In the line of multi-scale architectures, Yari et al. [24] first explored multi-scale contour detection CNNs for the purpose of firm layer extraction. The authors noted that using popular pre-training strategies would not work on Snow Radar images due to the inherent noise present in these images. Further extensions of [5] and [25] showed the usefulness of multi-scale architectures on synthetic radar images and temporal transfer learning, respectively. Subsequently, wavelet based multi-scale architectures for firm layer tracking were first developed in [23] which showed preliminary results in this domain. This prior work used a VGG-13 architecture [32] on a Snow Radar dataset, which comprised of both wet and dry snow zones, and achieved an F-score of little over 0.7. We expand upon this work by training a VGG-16 architecture, which is known to give robust representations [5], on a new dataset mostly consisting of dry zone images, where the firm layers can be tracked. Apart from further calculating the individual layer depths (in terms of number of pixels), we also show that using wavelet transforms of each scale of a multi-scale network helps in learning inherent image features, as compared to using multi-level wavelet transforms of the input image.

B. CNNs with Wavelet Transformations

Many recent works have tried to replace convolutional or pooling layers in a CNN with wavelet transform layers, such as in [16], [20], [11], [21], and [19]. [20] showed that using wavelet transform for downsampling would create much cleaner and sharper images, as compared to using pooling layers for the same purpose. Similarly, [16] found that wavelet transforms not only enlarge a kernel’s receptive field, but also prevent information leakage which generally takes place during a pooling operation. By using multi-level wavelet transforms, [21] developed deep convolutional framelets to reconstruct sparse-view computed tomography images and

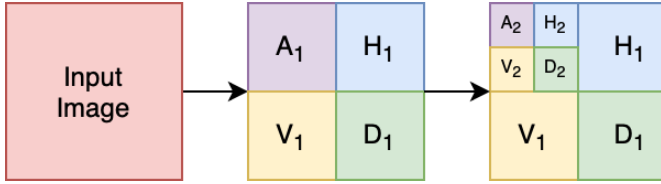


Fig. 1: A level 2 wavelet transform of a given input image. The subscript denotes the level number.

[11] developed a wavelet based loss function to super-resolve facial images. Further, [19] showed that residual learning improves by training on wavelet subbands. The variety of these works show that by incorporating wavelet transforms in a CNN, the feature extraction capability of the latter improves due to sharper feature maps, increased receptive field, and enhanced residual learning.

III. METHODOLOGY

In this section, we briefly explain the background of wavelet transforms, describe our base architecture without wavelets called Multi-Scale CNN, and then explain the wavelet combined neural networks for firm layer tracking.

A. Wavelet Transform

We use the Discrete Wavelet Transform (DWT) for our computations. For an image $f(x, y)$ having dimensions $X \times Y$, DWT is given as Equations 1 and 2 for $j \geq j_0$:

$$W_\phi(j_0, m, n) = \frac{1}{\sqrt{X \cdot Y}} \sum_{x=0}^{X-1} \sum_{y=0}^{Y-1} f(x, y) \phi_{j_0, m, n}(x, y) \quad (1)$$

$$W_\psi^i(j, m, n) = \frac{1}{\sqrt{X \cdot Y}} \sum_{x=0}^{X-1} \sum_{y=0}^{Y-1} f(x, y) \psi_{j, m, n}^i(x, y) \quad (2)$$

In these equations, W_ϕ is the approximation coefficient (A), and W_ψ^i are the detail coefficients for each level of wavelet transform j , where $i \in \{H, V, D\}$. H, V, D are the horizontal, vertical, and diagonal details, respectively, m, n are the subband dimensions [33], and j_0 is an arbitrary starting level. Each subsequent level of wavelet transform is computed on the previous level's approximation coefficient. In the beginning, the input raw image is treated as an approximation coefficient. Further, ϕ is a scaling function, and ψ is the wavelet function, both of which downsample an input image by a factor of 2 in both X and Y dimensions. Readers are encouraged to go through [34] to get a detailed understanding of ϕ , ψ , and the wavelet basis functions. We use the downsampling property of wavelets and combine their transforms with the side outputs of multi-scale networks. Figure 1 shows a level 2 (i.e. $j = 2$) transform of an input image. In our work, we experiment with three popular discrete wavelets, i.e. Haar, Daubechies, and 'Discrete' Meyer. We will be abbreviating them as 'haar', 'db', and 'dmev' in subsequent sections for ease of reading. The wavelet functions (ψ) for the three wavelet types have been plotted in Figure 2.

B. Multi-Scale CNN (MS-CNN)

In this work, we use a multi-scale network built for contour detection [35], which was proven to be useful for firm layer tracking ([5], [24]). This is a VGG-16 network with the terminal fully connected layers and the last pooling layer removed. The final convolutional layers of every stage, right before the max pooling layer of every stage, are convolved with a 1×1 filter to generate what we call "side output(s)". Each side output is at a downsampled resolution of the previous stage's side output. All side outputs are finally upsampled through transposed convolutions, followed by cropping, to match the resolution of the input image. The five side outputs, from the five stages, are concatenated together to form a 'fuse' layer. All five side outputs along with the final 'fuse' layer are trained together in a deeply supervised manner [36] with a cumulative loss function, Equation 5, as explained in the following paragraph.

To train the network, we calculate the binary cross entropy loss (l) for every pixel i as follows:

$$l(x_i; W) = \begin{cases} \alpha \cdot \log(1 - x_i) & \text{if } y_i = 0 \\ \beta \cdot \log(x_i) & \text{if } y_i = 1 \end{cases} \quad (3)$$

In Equation 3, x_i is the sigmoid activation map obtained from a network with weights W , y_i is the ground truth label of the corresponding pixel in the input image I having a total of $|I|$ pixels, and α, β are defined as Equation 4.

$$\alpha = \lambda \cdot \frac{|Y^+|}{|Y^+| + |Y^-|} \quad (4)$$

$$\beta = \frac{|Y^-|}{|Y^+| + |Y^-|}$$

In Equation 4, $|Y^+|$ denotes the count of all positive labels, i.e. those pixels representing the top of a layer ($y_i = 1$) and $|Y^-|$ denotes the count of all negative labels i.e. all other pixels which are background ($y_i = 0$). λ is a hyperparameter used to balance these positive and negative labels.

The total loss is computed as Equation 5 where k depicts each of the side outputs or stages, i.e. $K = 5$. This network, called Multi-Scale CNN, is the current state-of-the-art model for firm layer tracking [5] and forms our baseline architecture to compare with our wavelet-based architectures. Multi-Scale CNN is shown in Figure 3 and most of the times abbreviated as MS-CNN for the rest of the paper.

$$L(W) = \sum_{i=1}^{|I|} \left(\sum_{k=1}^K l(x_i^k; W) + l(x_i^{fuse}; W) \right) \quad (5)$$

C. Wavelet combined Neural Networks

We set up two wavelet based architectures, and exploit the multi-level nature of wavelet transforms to embed them into the base multi-scale architecture, MS-CNN. The two wavelet based network modifications are termed as 'WaveNet' and 'Skip-WaveNet', and described below:

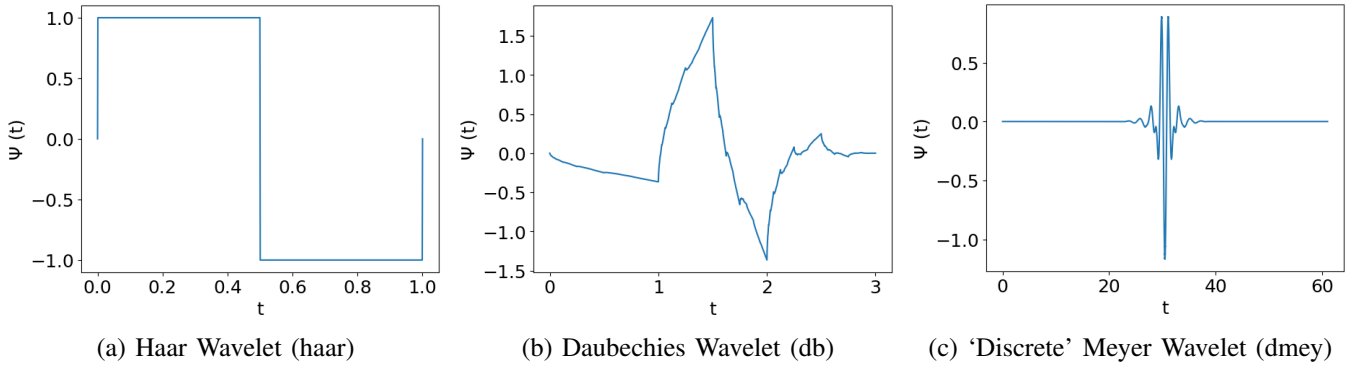


Fig. 2: The three types of wavelets that we use for our experiments

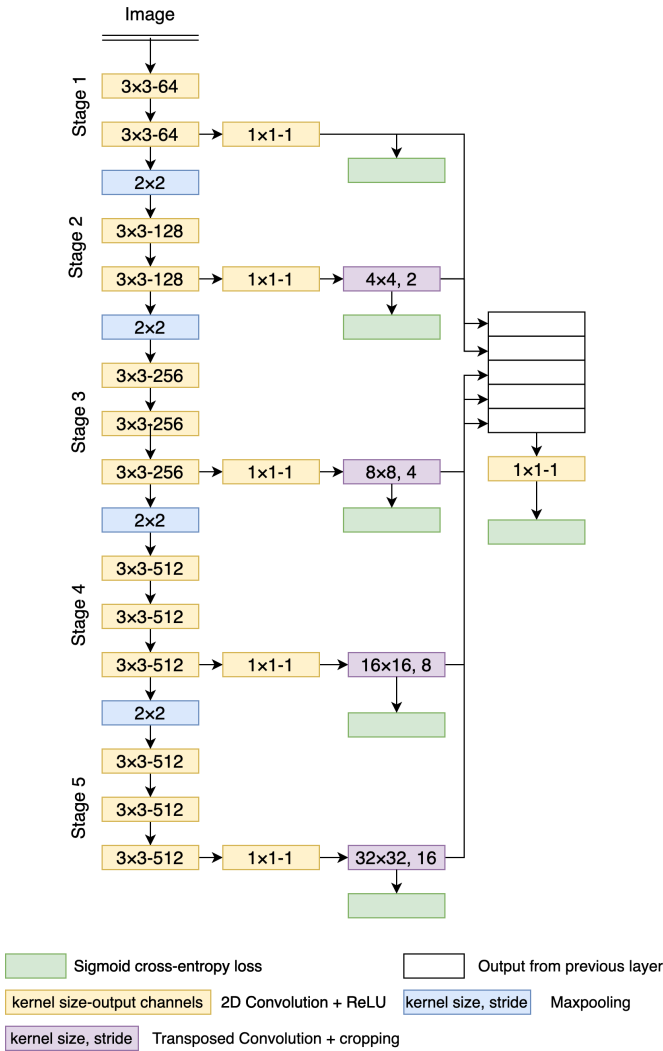


Fig. 3: MS-CNN - The multi-scale architecture [5] which forms our base model.

1) *WaveNet*: In Figure 3, from stage 2 to 5 of the base architecture, the feature maps get downsampled to a scale of 2x to 16x (with respect to the input image) to form the side outputs. Multi-level wavelet transforms of the input image also give us downsampled features at similar scales, which are sharp, denoised, and contain the horizontal, vertical, and

diagonal detail coefficients (see subsection III-A). By fusing wavelet information of the image to every scale, local as well as global, of the multi-scale network, the side outputs can be enriched for feature extraction. Hence, in this architecture, we take a level 4 wavelet transform (since there are four stages which have downsampled resolution as compared to the input image - stages 2 to 5) of the input image and fuse the detail coefficients in the following manner: we concatenate all three detail coefficients i.e. H, V, D of a wavelet transform of level l of the input radar echogram to the side output $l + 1$ of the base architecture. This means that the detail coefficients from level 1 of the wavelet transform fuse with side output 2 of the architecture, detail coefficients from level 2 of the wavelet transform fuse with side output 3 of the architecture, and so on. The WaveNet architecture is shown in Figure 4 .

2) *Skip-WaveNet*: The side outputs of MS-CNN are feature maps containing image patterns extracted at different scales, from local to global. These feature maps contain an improved representation of the features, i.e. are 'more learned', after every iteration of training and also contain noise in the form of unuseful network weights. Hence, they have a potential to be denoised further which can add value to overall network training. So for the Skip-WaveNet architecture, we take a wavelet transform of each side output and add it as an extra layer to the successive side output to supplement network learning. This will help form skip connections, support residual learning [19], [37] and also propagate information between scales. Since the wavelet transform is at a downsampled resolution to its input signal, the dimensions of a transform of side output s will be the same as the dimensions of side output $s + 1$. Further, by fusing the wavelet transform of a scale to its successive scale, we are also propagating information between scales which can support network learning. With this intuition, we form the Skip-WaveNet architecture as follows: we take a level 1 wavelet transform of a side output s ($s \in [1, 4]$) and fuse its detail coefficients to side output $s + 1$. In this case, for a given input image, the wavelet transforms will be renewed after each epoch of training. This can be compared against the WaveNet architecture where the transforms generated for an input image will be the same during all epochs. Hence, such multi-scale 'dynamic' wavelets should improve the denoising and feature extraction capabilities of the network. The architecture of Skip-WaveNet is shown in Figure 5 .

Apart from the above defined modifications, WaveNet and Skip-WaveNet are trained in the same way as the base architecture MS-CNN, i.e., they are trained with deep supervision through binary cross entropy loss, and have the final fusion of five side outputs, etc.

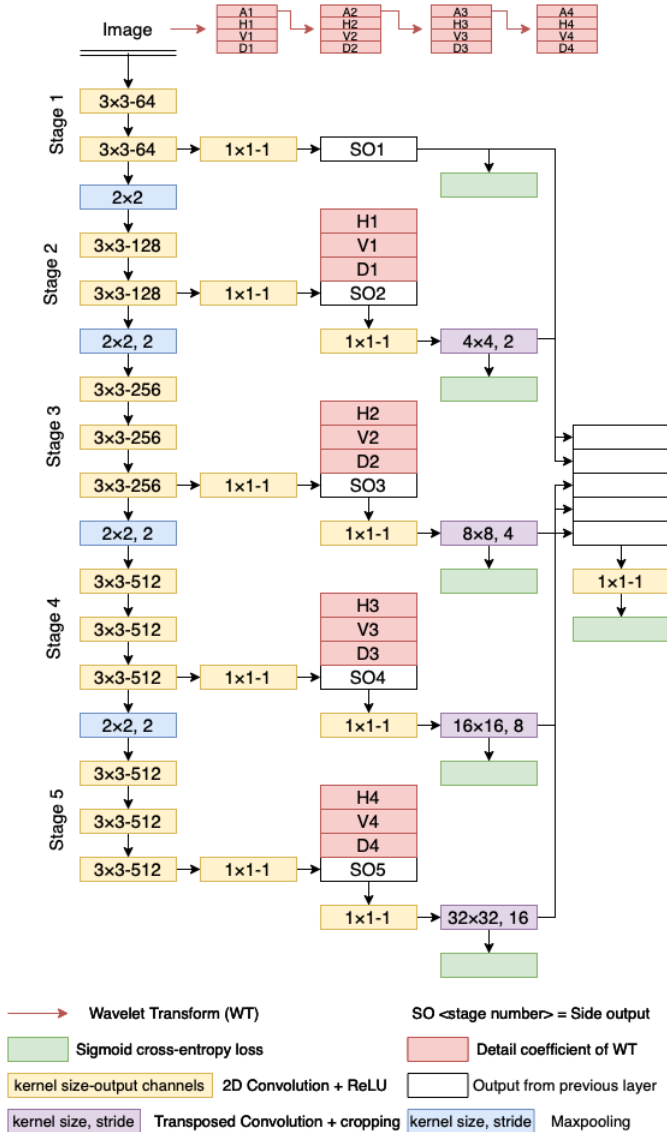


Fig. 4: WaveNet - A wavelet based architecture. Here wavelet transform is of the input image.

D. Experimental Setup

All the architectures, including the base architecture, and wavelet combined neural networks share the same hyperparameters as those used in [35] and [5]. For our experiments, we augment the training dataset with scaling factors $\in [0.25, 0.5, 0.75]$ and a left-to-right flipping. The augmentation helps in expanding the training dataset to 6430 images, which we train for 15 epochs. All networks took approximately 10 hours, on an average, when trained on NVIDIA GeForce RTX 2080 Ti GPU with an Intel Core i9 processor.

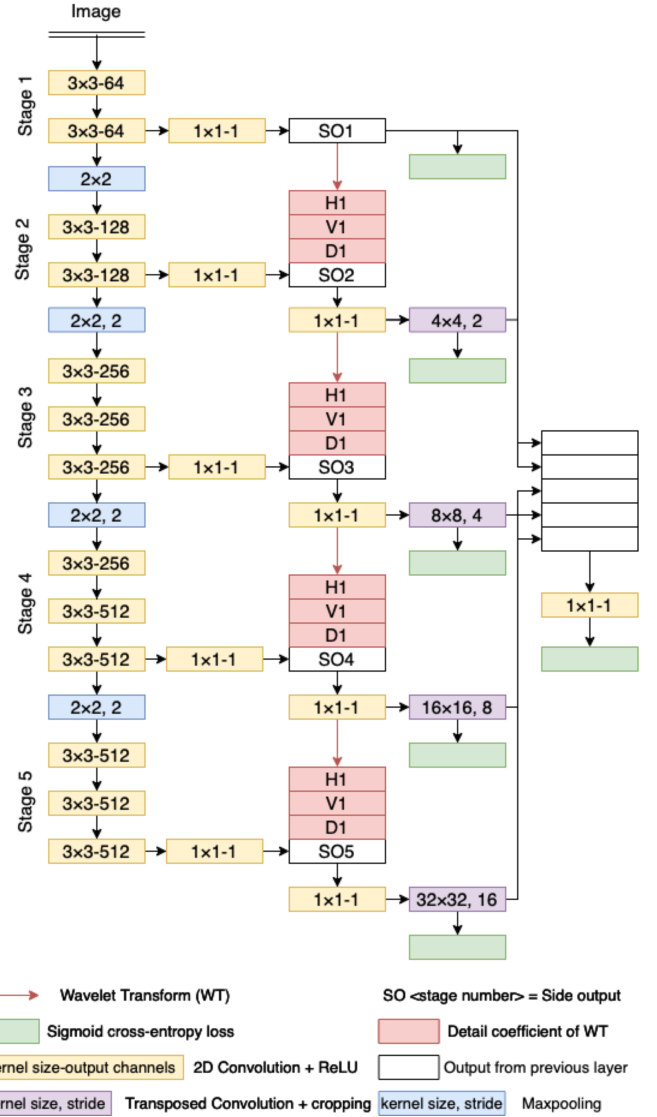


Fig. 5: Skip-WaveNet - A wavelet based architecture. Here wavelet transform is of each side output.

E. Post-processing and Evaluation

We perform non-maximum suppression (NMS) on the network outputs to make finer predictions of the layers. NMS gives grayscale predictions, which we compare against our ground truth by evaluating the ODS (optimal dataset scale) and OIS (optimal image scale) F-scores [38]. The ODS F-score looks for a single threshold across the entire dataset which can binarize the predicted image, and give the most optimum F-score with respect to the ground truth. On the other hand, OIS F-score searches for a similar optimum threshold for each image. The optimum F-scores thus found from each image are then averaged over the entire dataset to obtain the OIS F-score. Here, F-score refers to the standard F1-score used in computer vision, defined as Equation 6. In this equation, TP, FP, and FN are True Positives, False Positives, and False Negatives, respectively. We also use average precision (AP), which is the area under a precision-recall curve [39], as an evaluation metric of network performance.

$$F = \frac{TP}{TP + \frac{1}{2}(FP + FN)} \quad (6)$$

Based on the optimum threshold we get, we binarize the network outputs to get predictions similar to the ground truth. We then calculate the row indices (or the “range bin” indices of an echogram) of each layer in the predicted image matrix, and compare it with corresponding row indices of the manually labelled ground truth to evaluate the mean absolute error (MAE) of layer depth, Equation 7.

The mean row index of each layer gives us its depth in terms of number of pixels which can be used to calculate the distance between two successive layers. This gives us the layer thickness of the top layer in each pair of successive layers. Due to discontinuities in the ground truth layers, we perform minor corrective measures in our MAE evaluation, such as skipping any layer which is majorly (>50%) incomplete or imputing the mean of available row indices otherwise.

$$MAE = \frac{1}{T} \sum_{k=1}^{k=T} \frac{\sum_{j=1}^{j=N_k} \sum_{i=1}^{i=W_k} |GTD_i^{k,j} - PD_i^{k,j}|}{W_k \times N_k} \quad (7)$$

In Equation 7, GTD , and PD are the ground truth and predicted layer depths, respectively, in terms of number of pixels. For example, $PD_i^{k,j}$ represents the the row index of the j^{th} predicted layer in the i^{th} column of echogram k . W_k and N_k respectively represent the total number of columns (width), and the total number of traced layers, in echogram k . T represents the total number of echograms in the test set.

IV. DATASET

We use Snow Radar images publicly hosted by the Center for Remote Sensing and Integrated Systems (CRISIS) [40]. This dataset was captured over different regions of the GrIS [3] as shown in Figure 6. We clean this dataset by removing some of the images captured over the coast, to obtain 1286 training images and 321 test images. The images have a vertical resolution of approximately 4 cm per pixel, and each image has an along-track resolution of 14.5 m (Table I). We use binary labels for training and evaluation, where the top of each firn layer is labelled as ‘1’, and all other pixels are labelled as ‘0’. These labels are prepared manually by scientific experts tracing out the echograms through visual inspection.

TABLE I: Key parameters of the Snow Radar sensor used for data collection

Parameter	Value
Bandwidth	2-8 GHz
Pulse duration	250 μ s
PRF	2 kHz
Transmit power	100 mW
Intermediate frequency range	62.5 -125 MHz
Sampling frequency	125 MHz
Range resolution	\sim 4 cm
Along-track resolution	14.5 m

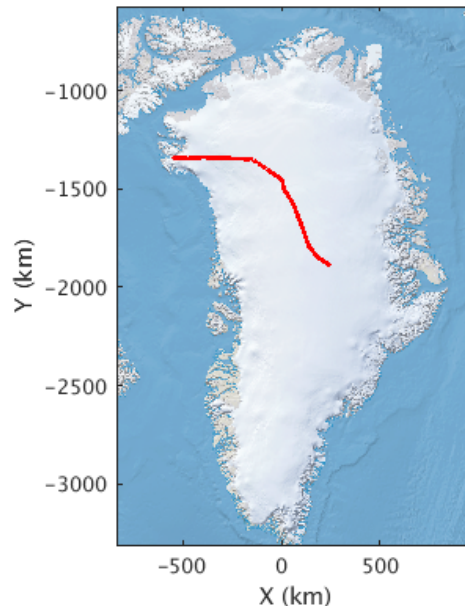


Fig. 6: Flight map of NASA Operation IceBridge 2012 in red, highlighting the regions of Greenland Ice Sheet over which the data was collected.

Network	Wavelet	ODS	OIS	AP	MAE
CNN3B+RNN [26]	None	NA	NA	0.853	8.730
	None	0.852	0.866	0.918	9.492
WaveNet	haar	0.876	0.888	0.936	3.517
	db	0.870	0.883	0.931	3.541
	dmey	0.835	0.851	0.905	3.967
Skip-WaveNet	haar	0.880	0.892	0.938	3.451
	db	0.879	0.890	0.937	3.438
	dmey	0.886	0.898	0.943	3.309

TABLE II: Evaluation metrics obtained across different model architectures on our test set. Highest scores highlighted in bold.

V. RESULTS AND DISCUSSION

We note that training with all five side outputs of our base MS-CNN model on the new dry-zone dataset by CRISIS is detrimental to performance, since there are hardly any global features or contours that this network (or humans in general) can detect (see for example, the radar echograms in Figures 8 and 9). Hence, we use only the first four side outputs and the fuse layer to train the baseline MS-CNN model. This is not the case for wavelet combined neural networks which are able to detect layer-contours across all scales, and can generate the fifth side output as well, capturing global context. In this section, we showcase our results on wavelet combined neural networks vs the baseline model, and also discuss about the wavelet architectures WaveNet vs Skip-WaveNet. We also compare our performance with the only other work on Snow Radar layer tracing [26].

A. Wavelet combined neural networks vs MS-CNN

We tabulate the ODS and OIS F-scores, the average precision (AP), as well as the mean absolute error (MAE) of depth

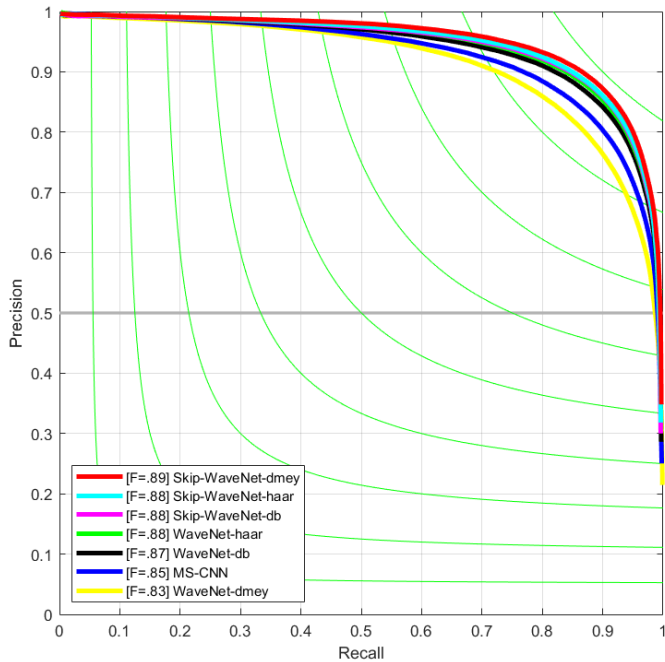


Fig. 7: Precision recall curves of different architectures over the test set.

estimates in Table II. These estimates are calculated on the final fuse layer of our experiments.

From Table II, we see that all wavelet combined neural networks, except for WaveNet with a dmey wavelet, perform better than the baseline MS-CNN model; which is also shown in the precision recall curves of Figure 7. The wavelet based networks also give higher AP and MAE scores (3.31 pixels) as compared to CNN3B+RNN [26]. Authors of CNN3B+RNN [26] were able to predict the top four to six layers from an echogram, while the multi-scale architecture, whether MSCNN or wavelet-based, can trace out the deeper, twenty to thirty, layers from the echogram (Figures 8-10).

In the wavelet-based networks the Skip-WaveNet with a dmey wavelet achieves the highest F-scores, with all Skip-WaveNet models performing better than WaveNet. The wavelet transforms help in improving the ODS F-score by 2.11%-3.99% and the OIS F-score by 1.96%-3.7%, over the baseline architecture, for different experiments. Thus, the wavelet transforms not only help in denoising feature maps, but also extract features at the global scale (fifth stage), which the comparative MS-CNN does not. Since images are extremely noisy (see the sample radar echograms in Figures 8-10), and the layers almost impossible to see by human eyes, this is a useful property that the wavelet architectures have achieved. Further, it should be noted that the number of *trainable* parameters in all architectures is the same.

Figures 8-10 showcase some of the qualitative results from the test set. As can be seen from these figures, the layers detected by the wavelet network are much “cleaner” than the baseline MS-CNN model. The baseline model is misguided by a lot of noise present in the input radar echograms, and falsely classifies certain backscatterings as a layer, as can be seen by

its intermediary predictions in between two layers. Further, a lot of the predicted layers are either broken, or have missing parts.

B. Skip-WaveNet vs WaveNet

Our experiments confirm that wavelet based architectures, by denoising echograms and enhancing feature extraction, are helpful for our use case. Hence we extend our quantitative analysis to Figure 11 where we compare the performance of the two wavelet architectures. In order to make a fair comparison, we evaluate the predictions results obtained on each side output (i.e. at each scale) and show the ODS F-scores in Figure 11. From this figure we see that Skip-WaveNet architecture gives a higher F-score across each scale (except for side output 1) and each type of wavelet, as compared to the WaveNet architecture. Thus, Skip-WaveNet is a more useful network, where the wavelet transform obtained in each epoch is from a learned and improved side output (so the wavelets are ‘dynamic’ and change after each epoch), whereas in WaveNet, the multi-level wavelet transforms are always fixed for a given input image for every epoch (the wavelets are in a way ‘static’ across the entire training period). We further see that the performance of the WaveNet experiment deteriorates with the wavelet complexity, whereas the performance of Skip-WaveNet improves with wavelet complexity (ODS F-score of dmey > db > haar). What would be interesting for future studies is to investigate is how the different types of wavelets are affecting network learning in different ways.

VI. CONCLUSION

Radar echograms are used for capturing the profile of multiple firm layers present on top of an ice sheet. These echograms can have varying characteristics, which we collectively refer to as “noise”, that can make firm layers difficult to detect visually or through automated algorithms. In this work, we use multi-level wavelet transforms and combine them with a multi-scale architecture to detect firm layers as contours. Our novel architecture helps in improving layer detection from noisy echograms. We also find that using wavelet transforms of intermediate side outputs and forming skip connections with them help in feature extraction and network learning, as compared to using ‘static’ wavelets of the input radar echogram. We believe that our algorithm can be used for internal layer tracking on any echogram created from a radar with sufficiently large bandwidth and fine vertical resolution such that the snow layers can be discriminated. The architecture can also be fine-tuned on newly acquired radar data from different radars such as the depth sounder sensor to achieve even better performance. Furthermore, a detailed analysis of how each type of wavelet function and its detail coefficient is contributing to the different architectures will enrich the field of signal processing.

REFERENCES

- [1] V. Masson-Delmotte, P. Zhai, A. Pirani, S. Connors, C. Péan, S. Berger, N. Caud, Y. Chen, L. Goldfarb, M. Gomis, M. Huang, K. Leitzell, E. Lonnoy, J. Matthews, T. Maycock, T. Waterfield, O. Yelekçi, R. Yu,

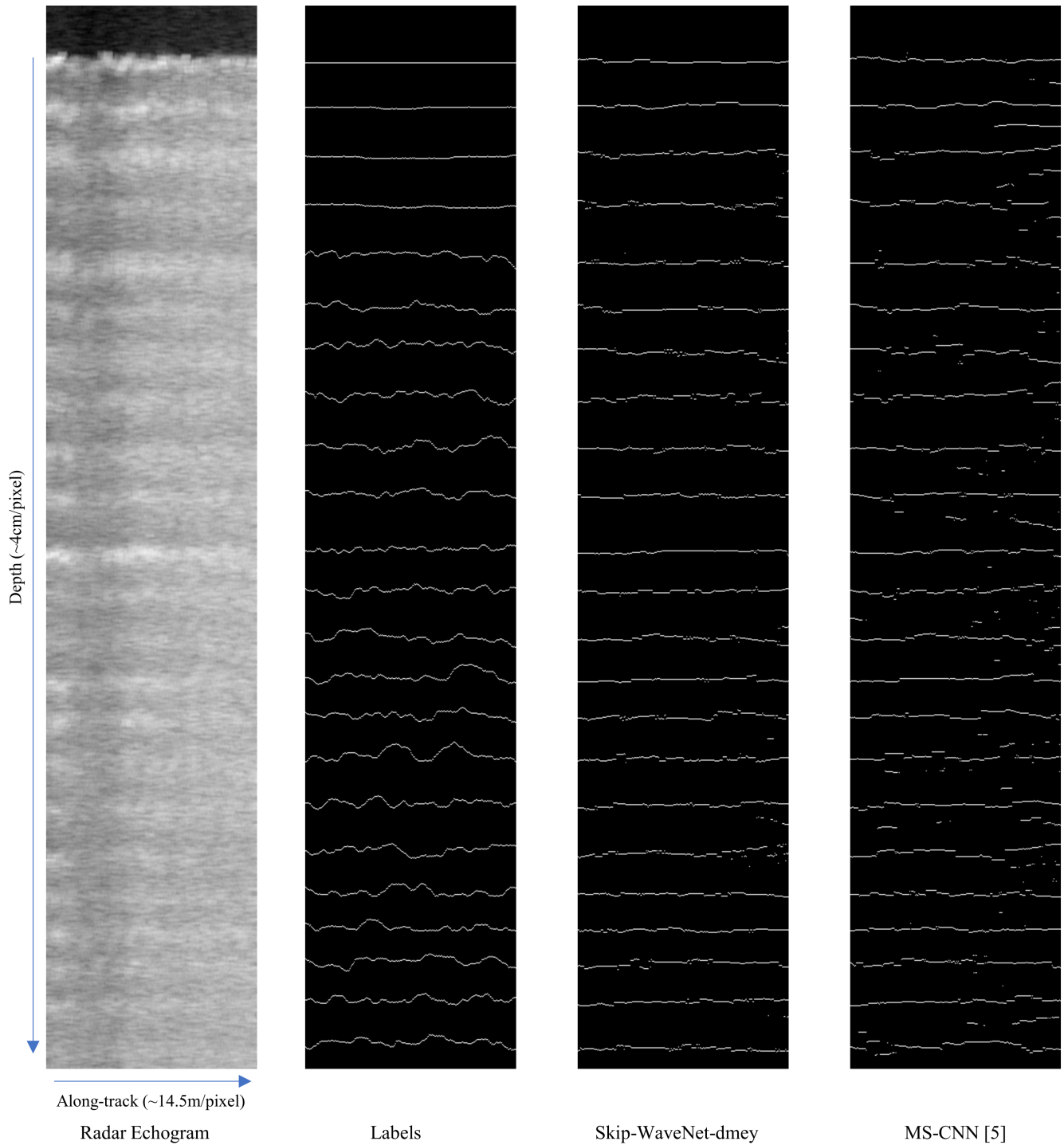


Fig. 8: Qualitative comparison of model outputs. From left to right, are the Snow Radar echogram, the ground truth labels, output by our Skip-WaveNet-dmey model, and output by Multi-Scale CNN [5].

and B. Z. (eds.), “Climate Change 2021: The Physical Science Basis. Contribution of Working Group I to the Sixth Assessment Report of the Intergovernmental Panel on Climate Change,” Intergovernmental Panel on Climate Change (IPCC), Tech. Rep., 2021.

[2] E. Kirezci, I. R. Young, R. Ranasinghe, S. Muis, R. J. Nicholls, D. Lincke, and J. Hinkel, “Projections of global-scale extreme sea levels and resulting episodic coastal flooding over the 21st Century,” *Scientific reports*, vol. 10, no. 1, pp. 1–12, 2020.

[3] L. S. Koenig, A. Ivanoff, P. M. Alexander, J. A. MacGregor, X. Fettweis, B. Panzer, J. D. Paden, R. R. Forster, I. Das, J. R. McConnell *et al.*, “Annual Greenland accumulation rates (2009–2012) from airborne snow radar,” *The Cryosphere*, vol. 10, no. 4, pp. 1739–1752, 2016.

[4] S. Gogineni, J. B. Yan, D. Gomez, F. Rodriguez-Morales, J. Paden, and C. Leuschen, “Ultra-wideband radars for remote sensing of snow and ice,” in *IEEE MTT-S International Microwave and RF Conference*, 2013, pp. 1–4.

[5] M. Rahnemoonfar, M. Yari, J. Paden, L. Koenig, and O. Ibikunle, “Deep Multi-Scale Learning for Automatic Tracking of Internal Layers of Ice in Radar Data,” *Journal of Glaciology*, vol. 67, no. 261, pp. 39–48, 2021.

[6] Y. LeCun, Y. Bengio, and G. Hinton, “Deep learning,” *nature*, vol. 521, no. 7553, pp. 436–444, 2015.

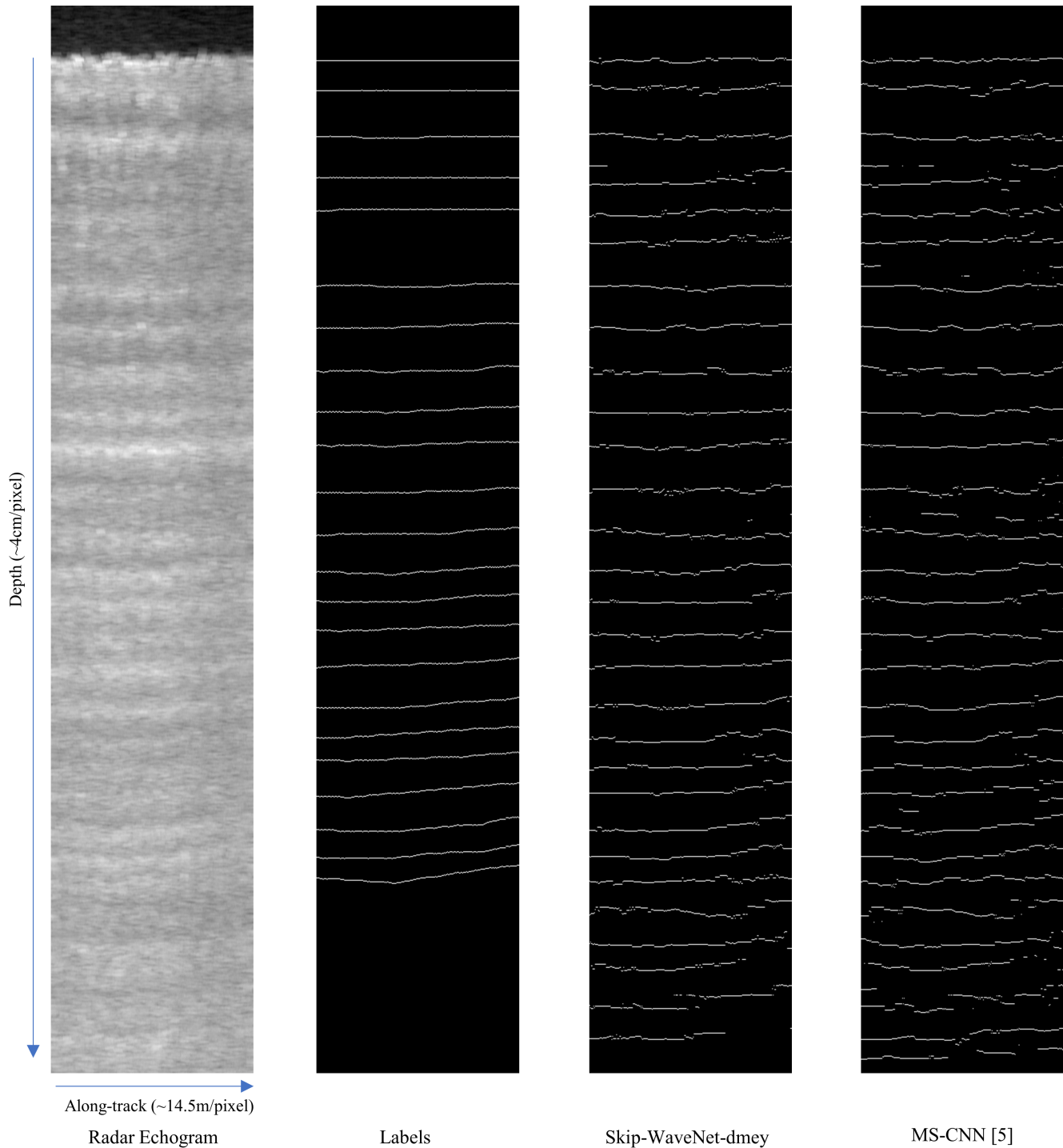


Fig. 9: Qualitative comparison of model outputs. From left to right, are the Snow Radar echogram, the ground truth labels, output by our Skip-WaveNet-dmey model, and output by Multi-Scale CNN [5].

- [7] D. Varshney, M. Rahnemoonfar, M. Yari, and J. Paden, "Deep Ice layer Tracking and Thickness Estimation using Fully Convolutional Networks," in *2020 IEEE International Conference on Big Data (Big Data)*. IEEE, 2020, pp. 3943–3952.
- [8] D. Varshney, M. Rahnemoonfar, M. Yari, J. Paden, O. Ibikunle, and J. Li, "Deep Learning on Airborne Radar Echograms for Tracing Snow Accumulation Layers of the Greenland Ice Sheet," *Remote Sensing*, vol. 13, no. 14, 2021. [Online]. Available: <https://www.mdpi.com/2072-4292/13/14/2707>
- [9] Q. Li, L. Shen, S. Guo, and Z. Lai, "WaveCNet: Wavelet Integrated CNNs to Suppress Aliasing Effect for Noise-Robust Image Classification," *IEEE Transactions on Image Processing*, vol. 30, pp. 7074–7089, 2021.
- [10] S. G. Mallat, "A Theory for Multiresolution Signal Decomposition: The Wavelet Representation," *IEEE Transactions on Pattern Analysis and Machine Intelligence*, vol. 11, no. 7, pp. 674–693, 1989.
- [11] H. Huang, R. He, Z. Sun, and T. Tan, "Wavelet-SRNet: A Wavelet-based CNN for Multi-scale Face Super Resolution," in *Proceedings of the IEEE International Conference on Computer Vision*, 2017, pp. 1689–1697.
- [12] K. Goyal and M. Mehra, "Fast diffusion wavelet method for partial differential equations," *Applied Mathematical Modelling*,

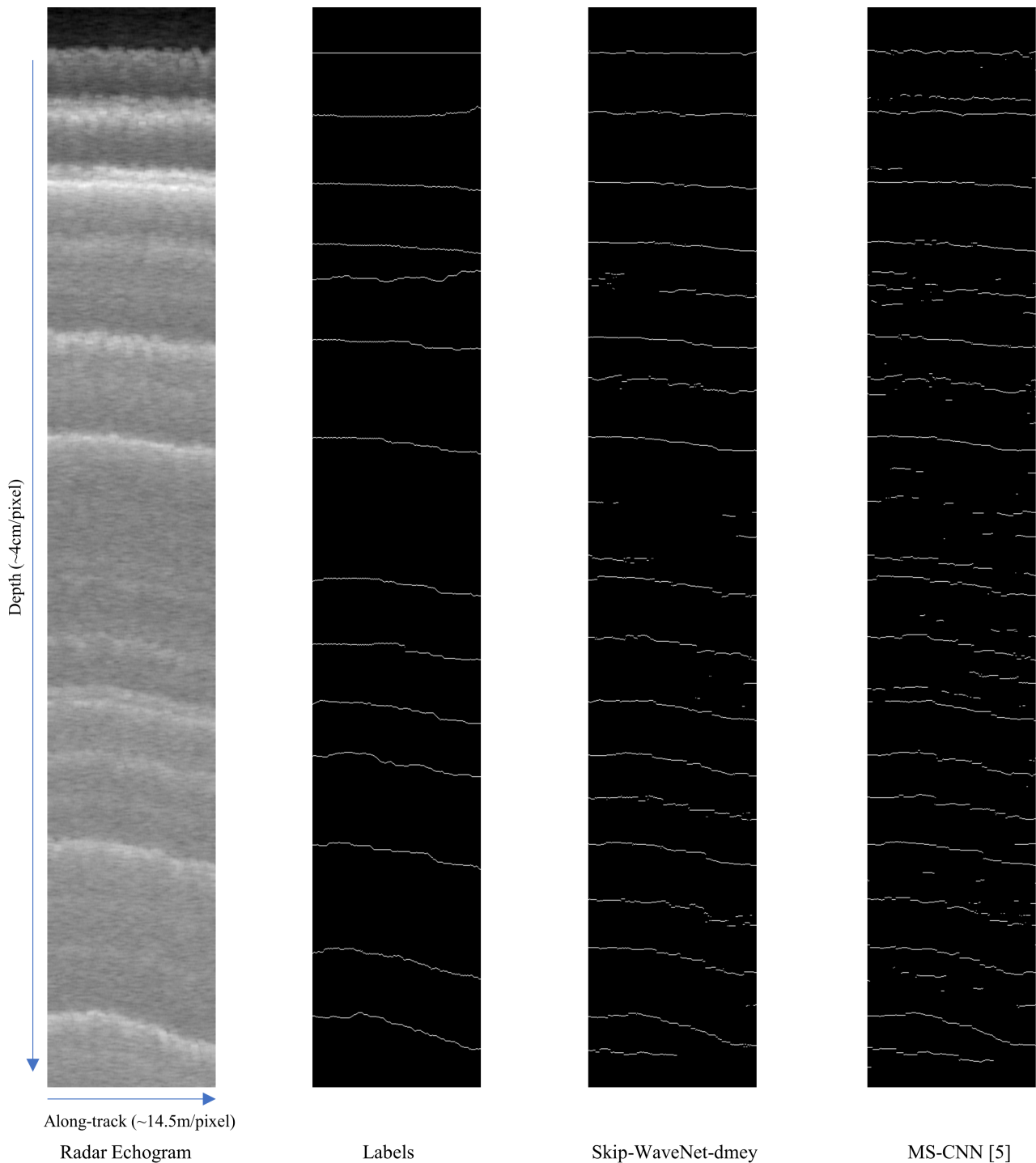


Fig. 10: Qualitative comparison of model outputs. From left to right, are the Snow Radar echogram, the ground truth labels, output by our Skip-WaveNet-dmey model, and output by Multi-Scale CNN [5].

vol. 40, no. 7, pp. 5000–5025, 2016. [Online]. Available: <https://www.sciencedirect.com/science/article/pii/S0307904X15007520>

[13] O. V. Vasilyev, D. A. Yuen, S. Paolucci, R. Gruber, and J. Rappaz, “Solving pdes using wavelets,” *Computers in Physics*, vol. 11, no. 5, pp. 429–435, 1997. [Online]. Available: <https://aip.scitation.org/doi/abs/10.1063/1.4822585>

[14] S. Mallat, “Understanding deep convolutional networks,” *Philosophical Transactions of the Royal Society A: Mathematical, Physical and Engineering Sciences*, vol. 374, no. 2065, p. 20150203, 2016. [Online]. Available: <https://royalsocietypublishing.org/doi/abs/10.1098/rsta.2015.0203>

[15] K. Bnou, S. Raghay, and A. Hakim, “A wavelet denoising approach based on unsupervised learning model,” *EURASIP Journal on Advances in Signal Processing*, vol. 2020, no. 1, pp. 1–26, 2020.

[16] P. Liu, H. Zhang, W. Lian, and W. Zuo, “Multi-Level Wavelet Convolutional Neural Networks,” *IEEE Access*, vol. 7, pp. 74973–74985, 2019.

[17] Z. Xiong and K. Ramchandran, “Chapter 18 - wavelet image compression,” in *The Essential Guide to Image Processing*, A. Bovik, Ed. Boston: Academic Press, 2009, pp. 463–493. [Online]. Available: <https://www.sciencedirect.com/science/article/pii/B9780123744579000184>

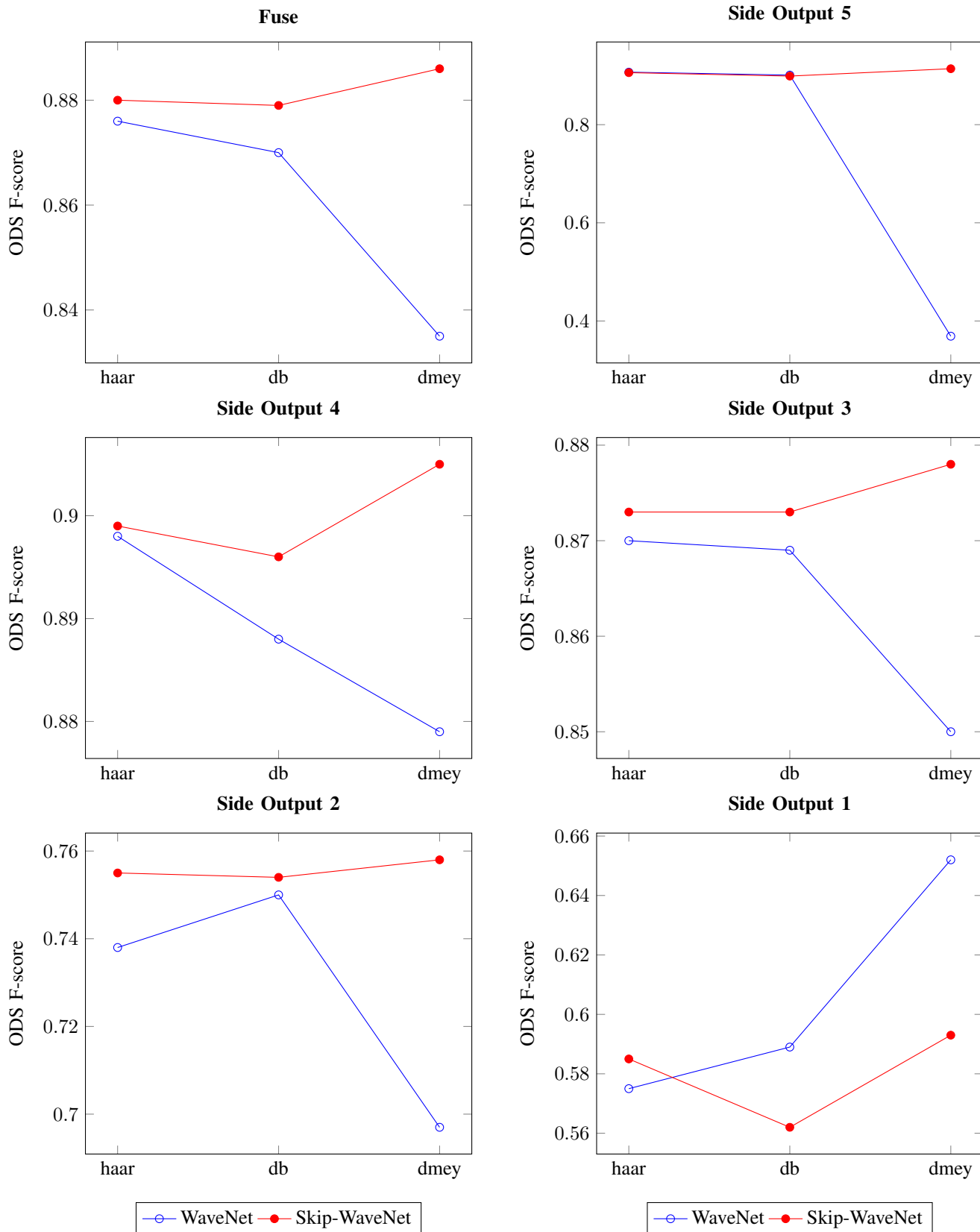


Fig. 11: The ODS F-score obtained at different scales of the network vs wavelet function for the two wavelet based neural networks.

- [18] R. Naveen Kumar, B. Jagadale, and J. Bhat, "A lossless image compression algorithm using wavelets and fractional Fourier transform," *SN Applied Sciences*, vol. 1, no. 3, pp. 1–8, 2019.
- [19] W. Bae, J. Yoo, and J. C. Ye, "Beyond Deep Residual Learning for Image Restoration: Persistent Homology-Guided Manifold Simplification," in *2017 IEEE Conference on Computer Vision and Pattern Recognition Workshops (CVPRW)*, 2017, pp. 1141–1149.
- [20] T. Williams and R. Li, "Wavelet Pooling for Convolutional Neural Networks," in *International Conference on Learning Representations*, 2018.
- [21] Y. Han and J. C. Ye, "Framing U-Net via Deep Convolutional Framelets: Application to Sparse-View CT," *IEEE Transactions on Medical Imaging*, vol. 37, no. 6, pp. 1418–1429, 2018.
- [22] O. Ronneberger, P. Fischer, and T. Brox, "U-Net: Convolutional Networks for Biomedical Image Segmentation," in *Medical Image Computing and Computer-Assisted Intervention – MICCAI 2015*. Springer International Publishing, 2015, pp. 234–241.
- [23] D. Varshney, M. Yari, T. Chowdhury, and M. Rahmehoonfar, "Refining Ice Layer Tracking through Wavelet combined Neural Networks," 2021. [Online]. Available: <https://www.climatechange.ai/papers/icml2021/49>
- [24] M. Yari, M. Rahmehoonfar, J. Paden, I. Oluwanisola, L. Koenig, and L. Montgomery, "Smart Tracking of Internal Layers of Ice in Radar Data via Multi-Scale Learning," in *2019 IEEE International Conference on Big Data (Big Data)*. IEEE, 2019, pp. 5462–5468.
- [25] M. Yari, M. Rahmehoonfar, and J. Paden, "Multi-Scale and Temporal Transfer Learning for Automatic Tracking of Internal Ice Layers," in *IGARSS 2020 - 2020 IEEE International Geoscience and Remote Sensing Symposium*, 2020, pp. 6934–6937.
- [26] Y. Wang, M. Xu, J. D. Paden, L. S. Koenig, G. C. Fox, and D. J. Crandall, "Deep Tiered Image Segmentation for Detecting Internal Ice Layers in Radar Imagery," in *2021 IEEE International Conference on Multimedia and Expo (ICME)*, 2021, pp. 1–6.
- [27] E. Donini, F. Bovolo, and L. Bruzzone, "A Deep Learning Architecture for Semantic Segmentation of Radar Sounder Data," *IEEE Transactions on Geoscience and Remote Sensing*, vol. 60, pp. 1–14, 2022.
- [28] R. Ghosh and F. Bovolo, "A Hybrid CNN-Transformer Architecture for Semantic Segmentation of Radar Sounder data," in *IGARSS 2022 - 2022 IEEE International Geoscience and Remote Sensing Symposium*, 2022, pp. 1320–1323.
- [29] —, "TransSounder: A Hybrid TransUNet-TransFuse Architectural Framework for Semantic Segmentation of Radar Sounder Data," *IEEE Transactions on Geoscience and Remote Sensing*, vol. 60, pp. 1–13, 2022.
- [30] A. Vaswani, N. Shazeer, N. Parmar, J. Uszkoreit, L. Jones, A. N. Gomez, L. u. Kaiser, and I. Polosukhin, "Attention is all you need," in *Advances in Neural Information Processing Systems*, I. Guyon, U. V. Luxburg, S. Bengio, H. Wallach, R. Fergus, S. Vishwanathan, and R. Garnett, Eds., vol. 30. Curran Associates, Inc., 2017. [Online]. Available: <https://proceedings.neurips.cc/paper/2017/file/3f5ee243547dee91fbd053c1c4a845aa-Paper.pdf>
- [31] O. Ibikunle, J. Paden, M. Rahmehoonfar, D. Crandall, and M. Yari, "Snow Radar Layer Tracking Using Iterative Neural Network Approach," in *IGARSS 2020 - 2020 IEEE International Geoscience and Remote Sensing Symposium*, 2020, pp. 2960–2963.
- [32] K. Simonyan and A. Zisserman, "Very Deep Convolutional Networks for Large-Scale Image Recognition," in *International Conference on Learning Representations*, 2015.
- [33] T. Williams, R. Li *et al.*, "An Ensemble of Convolutional Neural Networks Using Wavelets for Image Classification," *Journal of Software Engineering and Applications*, vol. 11, no. 02, p. 69, 2018.
- [34] I. Daubechies, *Ten Lectures on Wavelets*. Society for Industrial and Applied Mathematics, 1992. [Online]. Available: <https://epubs.siam.org/doi/abs/10.1137/1.9781611970104>
- [35] S. Xie and Z. Tu, "Holistically-Nested Edge Detection," in *2015 IEEE International Conference on Computer Vision (ICCV)*, 2015, pp. 1395–1403.
- [36] C.-Y. Lee, S. Xie, P. Gallagher, Z. Zhang, and Z. Tu, "Deeply-Supervised Nets," in *Artificial intelligence and statistics*. PMLR, 2015, pp. 562–570.
- [37] K. He, X. Zhang, S. Ren, and J. Sun, "Deep Residual Learning for Image Recognition," in *Proceedings of the IEEE conference on computer vision and pattern recognition*, 2016, pp. 770–778.
- [38] Y. Liu, M.-M. Cheng, X. Hu, J.-W. Bian, L. Zhang, X. Bai, and J. Tang, "Richer Convolutional Features for Edge Detection," *IEEE Transactions on Pattern Analysis and Machine Intelligence*, vol. 41, no. 8, pp. 1939–1946, 2019.
- [39] W. Su, Y. Yuan, and M. Zhu, "A Relationship between the Average Precision and the Area under the ROC Curve," ser. ICTIR '15. New York, NY, USA: Association for Computing Machinery, 2015, p. 349–352. [Online]. Available: <https://doi.org/10.1145/2808194.2809481>
- [40] CReSIS, "NASA OIB Greenland," 2012. [Online]. Available: https://data.cresis.ku.edu/data/temp/internal_layers/NASA_OIB_test_files/image_files/snow/OLD_2012_Greenland_P3/2012_Greenland_P3/frames_001_243_20120330_04/